Chapter 5

TOWARD HIGHLY SPECIFIC CONTROL OF BIOLOGICAL ACTIVITY USING TEMPERATURE-SENSITIVE PROTEIN TAGS

5.1: Toward Broader Implementations of TlpA-Based Bioswitches

Temperature-dependent bioswitches are poised to play a key role in a variety of applications of synthetic biology and biochemical engineering. In addition to their demonstrated ability to effect transcriptional control in response to both endogenous and exogenous thermal perturbations for cell therapy applications[1], they may also be utilized in industrial settings such as bacterial ghost production for vaccine development[2] and regulation of large-scale protein production[3]. The development of TlpA as a modular thermal bioswitch, as described in Chapter 4, enables a plethora of novel applications such as noninvasive control of protein function in living animals or potentially in cell-based human therapeutics. To realize this potential, TlpA-mediated thermal regulation must progress beyond proof-of-concept control of protein localization and demonstrate the ability to robustly modulate protein activity.

Biological systems for controlling protein-protein interactions via non-thermal mechanisms have been developed and may serve as templates for the expansion of the TlpA-controllable repertoire. Among the most famous of these strategies is the FKBP-based chemically inducible dimerization (CID) system developed by Crabtree and colleagues, which confers stable dimerization in the presence of the drug Rapamycin or derivatives thereof[4].

Subsequently, orthogonal CID systems based on ligands such as S-(+)-abscisic acid (ABA)[5] and a gibberellin derivative[6] have been developed. Recently, an antibody-based system for CID aimed at supporting cell therapy applications was introduced and may prove less immunogenic than previous technologies based on foreign proteins[7]. The broad implementation of CID for elucidating the behavior of biomolecules[8] has inspired optogenetic analogues such as the protein domain pairs Phy/PIF[9], FKF1/GI[10], and pMag/nMag[11], which combine the inducibility of their chemical predecessors with novel spatial and temporal axes of control. The wealth of previous work demonstrating the potential of inducible dimerization provides a roadmap along which the development of thermo-controllable dimerization agents can proceed. A variety of preliminary experiments have been conducted which may provide valuable insight for future TlpA engineering efforts.

5.2: Potential Approaches to High Resolution Structural Determination of TlpA

While previous work has suggested that TlpA consists of a globular N-terminal DNA binding domain and an elongated C-terminal coiled-coil[12,13], neither the atomic-resolution structure of the protein nor the mechanism for its uniquely sharp melting profile has been elucidated. Biological structure is intimately linked to function[14]; a detailed understanding of the atomic arrangement of TlpA may assist in both the determination of its enhanced switching profile relative to structurally similar proteins such as tropomysin[15,16], and also in the design of novel fusion proteins or orthogonally-dimerizing variants for multiplexed control.

The three main methods of biological structure determination are Nuclear Magnetic Resonance (NMR) spectroscopy, cryo-electron microscopy (Cryo-EM), and X-ray crystallography[17,18]. NMR structure determination is unique in its ability to sample proteins in their native aqueous environment[19]. However, the method is hampered by similarity in local chemical environments leading to chemical shift degeneracy in the spectra[20], which imposes a 30-50 kDa limit to the size of protein complexes amenable to this analysis. The TlpA dimer, consisting of two 41.5 kDa monomers, may be beyond the reach of this technique, particularly since the helical repeat structure of the coiled-coil results in high structural similarity along the length of the coil, further compressing the range of chemical environments and blending chemical shifts[21].

Cryo-EM, while reliant on flash freezing, also produces structures in a more native-like environment than crystallography. However, this method depends on imaging thousands of representative particles and averaging them to reconstruct an accurate high-resolution model. Previous low-resolution transmission electron microscopy images suggest that the length of TlpA may impart some conformational flexibility and that high expression of the protein may lead to packing into randomly arranged superstructures[22], both of which may impede reference averaging. A recent advance in Cryo-EM is the use of auxiliary scaffolding molecules to stabilize proteins structures while acting as fiducial markers for averaging, thereby enabling resolution of proteins which are too small to discern in isolation[23–25]. This methodology can be combined with the well-established capability of EM to visualize DNA origami superstructures[26]; in fact, intrinsically-disordered proteins of the nuclear pore have been characterized using this methodology, albeit at low resolution[27]. It is tempting to

imagine a DNA nanostructure containing the TlpA operator/promoter sequence implemented as a scaffold to stabilize protein conformation and enable EM-based structural characterization. Furthermore, if another DNA-binding domain can be attached to the C-terminus of TlpA, the protein could be stretched in an extended conformation inside of the DNA cage, thereby minimizing particle-to-particle structural variation.

The mainstay of structural biology to date has been X-ray crystallography. This method utilizes chemical perturbations administered in an empirically optimized fashion to generate proteinaceous crystals, the diffraction of which can be reconstructed into an electron density model. Crystallography can generate atomic resolution models of large proteins; notable solved structures include a 45 nm bundle consisting of 200-residue-helix fibrinogen monomers[28] (PDB 3GHG), an engineered 30 nm trimeric 300-residue coiled-coil containing a bacteriophage fiber gp26 protein[29] (PDB 4LIN), a similar 200-residue trimeric coiled-coil from phage HK620[30] (PDB 5BVZ), and the 40 nm dimeric coiled-coil tropomysin[31] (PDB 1C1G).

The crystallization process is poorly characterized and optimization varies on a protein-to-protein basis[32]. We have previously attempted to crystallize full length $TlpA^{1-371}$ and a truncated portion predicted to correspond to the coiled coil ($TlpA^{69-292}$) but all crystallization conditions from four 96-well screening plates (Hampton Research) produced non-crystalline aggregates. Challenges to crystallization included maintaining solubility at the requisite 10 mg/mL concentration, separation of the 80 kDa TlpA dimer from a 70 kDa contaminant protein which co-eluted with the desired product after histidine affinity purification, and

relatively low expression of the protein in soluble form (on the order of 1 mg per L of culture). A more focused structural study may employ tandem affinity, ion exchange, and size exclusion chromatography to obtain crystallographically pure samples of TlpA, and may also screen buffer conditions similar to those that enabled the previous determination of large alpha-helical proteins. Another potential strategy is fragment-based reconstruction in which the full length protein could be subdivided into smaller, potentially more soluble components. Finally, a DNA segment corresponding to the TlpA operator/promoter may bind to and stabilize the protein to enable crystallization[33].

5.3: Structural Inferences from Bioinformatics

In lieu of an atomic resolution structure, engineering efforts must be guided by bioinformatics and biochemical prediction. The current model of TlpA structure is guided by manual alignment of the primary amino acid sequence of the C-terminal domain with that of a prototypical coiled-coil heptad repeat motif[12], homology-based secondary structure prediction[13], circular dichroism spectroscopy suggesting high alpha-helical content[12,13,34], and the success of the rational introduction of heterodimerizing mutations informed by these predictions (Chapter 4). While these techniques hint at the general structural features of TlpA, they fail in two key respects. First, they do not provide insight into the mechanism of unique switching sharpness demonstrated by TlpA. Next, they fail to predict suitable locations for modification and functionalization of the protein.

The overall structure of TlpA is predicted to consist of an N-terminal globular domain followed by a C-terminal coiled coil, as predicted by manual annotation[12] and by three different software prediction packages. The linear structural prediction is summarized in **Fig. 5-1**, which aligns the secondary structure prediction assigned to TlpA by the software Jpred4[35] with the coiled-coil annotations ascribed by COILS[36], PairCoil2[37], and LOGICOIL[38], and also the manual annotation reported in the original publication by Koski et al[12]. It is evident that, while the C-terminal portion of the protein has a characteristic coiled-coil sequence as evidenced by its homology-based annotation, the per-residue register of the protein is not fully consistent with classical coiled-coil structure. The annotations from all three prediction servers demonstrate truncated heptad repeats and skips, which may indicate either failure of the homology-based algorithms to predict the possibility of the given residues at their respective positions in the coiled-coil structure, or deviations from the coiled-coil motif in the real protein structure. Such aberrations are interesting because they may influence the unique temperature-sensing abilities of TlpA. Previous studies have implicated breaks in predicted coiled-coil structure in influencing stability[39] or having other functional consequences such as binding of accessory proteins[40]. Understanding the fine details of the local structure at these positions is likely to aid in the elucidation of the thermo-sensing mechanism of this protein.

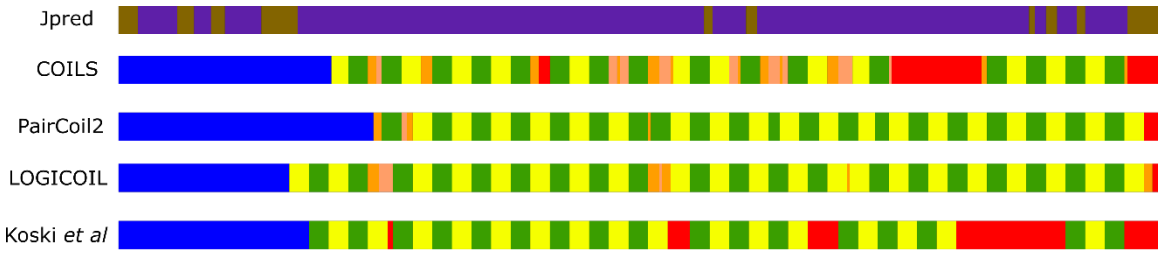

Figure 5-1: Sequence prediction annotation of TlpA. The primary sequence of TlpA is annotated by its predicted secondary structure (Jpred4, top) or for its predicted conformity to the characteristic heptad repeat pattern as described by the homology-based prediction software COILS, PairCoil2, and LOGICOIL, and as described in the initial report of the TlpA gene. In the Jpred4 prediction, brown segments indicate unstructured regions and purple blocks represent α-helices. In the coiled-coil predictions, the initial blue segments denote the N-terminal domain annotations and alternating yellow and green segments denote full heptad repeats. Orange and beige segments indicate regions which are predicted to be in a coiled-coil conformation but do not span for an entire heptad, indicating a shift in register. Red segments indicate predicted interruptions in the coiled-coil motif.

The initial discovery of TlpA was motivated in part by its sequence similarity to Tropomyosins (Tpm)s, which are elongated coiled-coil proteins (**Fig. 5-2a**) that regulate muscular contractions[41]. The sequence identity between TlpA and tropomyosins from various species ranges from 15.5 – 20.2%[12] and is clustered into three regions (**Fig. 5-2b**). While the sequence identity with TlpA is low even inside these clusters (**Supplementary Fig. 5-S1**), it is likely that the general structural heuristics of Tpm – that of an approximately 40 nm elongated parallel dimeric coiled-coil – are preserved in the TlpA protein. Both TlpA and Tropomyosin display relatively cooperative thermal unfolding compared to shorter leucine zippers, with 10%-90% dissociation ranges of 4-5 °C[34], 6-10 °C[16], and 20-25 °C[42] for TlpA, Tpm, and Fos/Jun, respectively. This length-dependent increase in coiled-coil folding cooperativity coincides with simulations predicting as such to a plateau of approximately 50 residues[43], a boundary between the lengths of Fos/Jun and the long TlpA and Tpm proteins. Nevertheless, the switching sharpness of TlpA is able to accommodate the transition between homeostatic temperature and mild hyperthermia (37 °C to 42 °C) whereas Tpm would be hard-pressed to unfold within this range, indicating that a structural feature unique to TlpA confers such cooperativity of unfolding. It is tempting to speculate that the break in predicted coiled-coil helical structure between two “coil islands” predicted by Koski et al, Jpred4, and COILS (**Fig. 5-1**) may enhance thermo-sensitivity, although these

predictions assign the interruptions to different positions within the primary sequence and as such are difficult to draw conclusions from. Interestingly, both TlpA and Tpm contain a singly cysteine residue which is known to be at the strand-strand interface, either from crystallographic data (Tpm) or its accessibility to $CuCl_2$-catalyzed oxidative crosslinking (TlpA). Interfacial cysteine residues have been implicated in redox sensing[44] and tropomyosin is known to be oxidized due to ROS formation upon myocardial infarction[45], which may inhibit its function in the sarcomere. While the function of the TlpA protein in its native context is unknown, and it is dispensable for the infectivity of the bacterium that carries it[46], the location of the *tlpA* gene in the virulence plasmid of Salmonella suggests a functional role in the host-pathogen interaction. It is known that Salmonella encounters an oxidative burst during macrophage uptake[47,48], suggesting a possible dual role for the protein in temperature and redox sensing. Previous work tracking TlpA auto-regulation demonstrated increased TlpA expression at 37 °C relative to 26 °C, and no increase in TlpA levels between 37 °C and 37 °C + 100 μM H_2O_2, but did not assay for expression at 26 °C +

H_2O_2 to determine if oxidative stress may sensitize the protein to de-repress its cognate promoter at a lower thermal threshold[46].

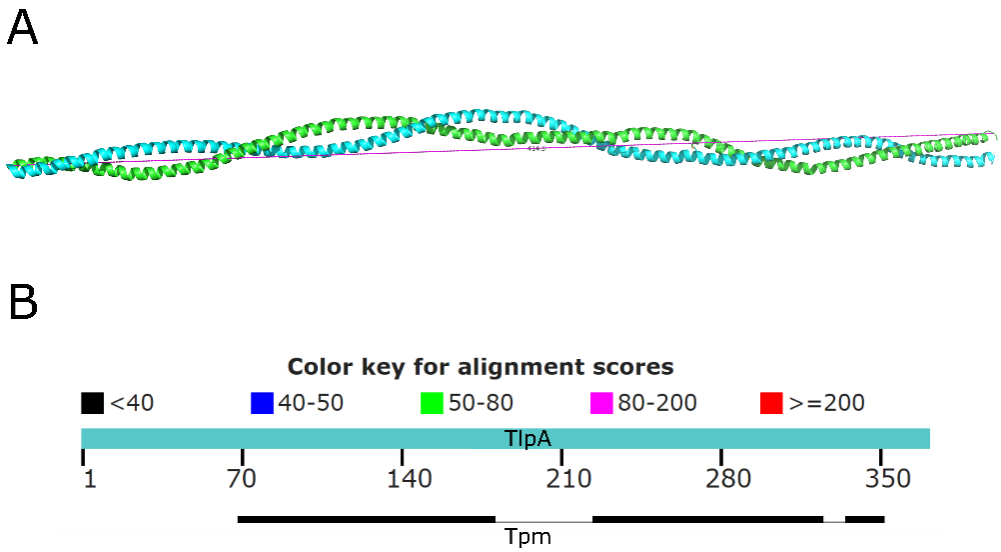

Figure 5-2: Structural similarity of TlpA to Tropomyosin. a) The crystal structure of an α-Tropomyosin dimer, a 284 residue 41 nm coiled-coil protein with relatively high homology to the TlpA coiled-coil domain (PDB 1C1G). **b**) Alignment of the TlpA protein sequence with that of α-Tropomyosin via the Basic Local Alignment Search Tool (BLAST).

5.4: Functional Inferences from Bioinformatics

The *tlpA* gene is found in the pSLT virulence plasmid of *Salmonella typhimurium*[46]. Previous characterization has demonstrated that the protein may be secreted by the bacterium via mechanisms other than direct cell-lysis, but it does not escape from endosomes into the host cytoplasm and as such this secretion may not be functionally relevant. Deletion of *tlpA* does not impact the infectivity or distribution of Salmonella during infection BALB/C murine hosts. It should be noted that this study did not measure the temperature of the mice after infection, and even direct LPS injection can produce only mild febrile response in BALB/C

mice[49], and that the thermal response is age-dependent[50]. As such, this result may not generalize to other scenarios of infection. However, the study did demonstrate TlpA activation upon transition from the external environment (26 °C) to host temperature (37 °C) *in vitro,* suggesting a functional role in this event. This thermal regime is lower than the biotechnological role for which we developed TlpA (sensation of hyperthermia above mammalian core temperature). This discrepancy may be explained by the low copy number of the pSLT virulence plasmid (1-2 plasmids per cell) compared to the >100 copy number of the ColE1-based plasmids utilized in our studies, in conjunction with the known concentration-dependence of the TlpA dissociation threshold[34].

Functional studies of TlpA have focused on its published role in auto-regulation via the 5'-3' promoter activity of the sequence directly upstream of the *tlpA* gene[34] (the TlpA operator/promoter). While TlpA auto-regulation certainly impacts the transcriptional set point of its own expression level, the fact that TlpA has not been deleted from the virulence plasmid suggests that it has an important functional role benefiting the bacteria, likely via additional TlpA-regulated components. One possibility is that TlpA binds to other cognate operator sequences within the virulence plasmid or in the bacterial chromosome; however, we were unable to find homologous sequences in either DNA molecule using BLAST alignment[51]. Another option is polycistronic regulation of one or more genes downstream of the TlpA repressor. We have demonstrated regulation in this fashion (see pThermeleon, Chapter 3). We have not performed experimental gene expression analysis of virulence plasmid-associated genes during infection, but the native context of TlpA positions the repressor upstream of another coding sequence in a manner which may enable polycistronic

regulation (**Fig. 5-3**). While the sequence between *tlpA* and the downstream ORF has not been annotated, we note that it contains an A/T-rich element (ATAAT) approximately 30 bp upstream of its start codon (roughly the same as the spacing between the TlpA promoter and the *tlpA* initiating methionine), implying that this UTR may itself function as a promoter. The downstream gene has high homology to YacC, a poorly-characterized periplasmic protein with unknown relevance to virulence[52]. Differential gene expression analysis of this YacC homologue upon heat shock can determine if the upstream TlpA regulates it in a polycistronic fashion. An alternative and intriguing possibility for the role of the TlpA system stems from our discovery that TlpA can function as a bidirectional promoter (Chapter 3, **Fig. 3-S2**). The reverse-complemented sequence upstream of the TlpA promoter contains an open reading frame in the correct orientation to be transcribed by reverse activity of the TlpA promoter (**Fig. 5-3**). Excitingly, the protein sequence of this gene bears high homology to YadA, an adhesin which serves as an essential virulence factor in several strains of *Yersinia*[53]. Future work may expand on the role of TlpA in regulating *Salmonella* infectivity, and particularly its putative function as a regulator of the native *yadA* homologue.

Figure 5-3: Endogenous sequence context of TlpA. Local sequence annotation of the *tlpA* locus on the pSLT virulence plasmid of *Salmonella typhimurium* (NCBI RefSeq NC_003277.1, bp 38,923 – 41,287).

5.5: Inferences from Structural and Functional Activity Assays

The TlpA-based platform for controlling gene expression, described in Chapter 3, can be utilized as a tool to investigate the functional outcomes of modifications to the TlpA repressor. While the requirement for an intact DNA binding domain limits the scope or perturbations accessible at the N-terminus of the protein, internal and C-terminal modifications may be freely examined. Comparison of reporter gene activation between circuits carrying the wild type *tlpA* gene and its derivatives can inform the role of some structural features, as well as the tolerance of the protein to modification at particular locations.

Analysis of deletions at the C-terminus demonstrates that, surprisingly, TlpA is highly sensitive to even small truncations in this region. **Fig. 5-4a** shows that even a 13 residue truncation, predicted by Koski et al to be outside of the coiled-coil region[12], greatly disrupts repression and cooperative dissociation of the repressor. The sensitivity of the TlpA C-terminus to modification is corroborated in **Fig. 5-4b** and **5-4c**, in which fusion of the anionic triplet Asp-Glu-Asp (DED) or a strongly cationic sequence (SV40 NLS) also results in disruption of activity. The addition of a short SLGSGS linker partially alleviates disruption, suggesting that proximity to the C-terminus is a factor in destabilization (**Fig. 5-4c**). This impediment of functionality is likely due to Coulombic repulsion between the like-charged residues symmetrically apposed between the two strands; partial charge neutralization via fusion of the cationic NLS sequence to the anionic DED motif alleviates the disruptive effect and even appears to stabilize the complex, possibly via charge cross-complementation (**Fig.**

5-4d). To examine the possibility of fusing protein domains to the TlpA C-terminus without inhibiting its function, we opted to screen hexahistidine tags as mild disruptive elements separated from the C-terminal residue of TlpA by a panel of flexible linkers (**Fig. 5-4e**). Three and five-residue linkers did not confer any stabilization over the no-linker condition. The fifteen-mer linker did alleviate destabilization at temperatures above 34.1 °C but appeared slightly de-repressed compared to unmodified TlpA at lower temperatures. In contrast, the 25-residue linker alleviated the disruptive effect of the His_6 tag at all temperatures tested. The L25 linker permits TlpA to tolerate the presence of a larger and more sterically hindered domain, the 40 kDa globular protein MBP (**Fig. 5-4f**). Similarly, while shorter linkers are unable to restore cooperative activation to C-terminal fusions of the SV40 NLS (**Fig. 5-4g**), the L25 linker restores tolerance for this modification, which even confers additional stability through an unexplored mechanism (**Fig. 5-4h**). The a79 NLS[54], which contains fewer charged residues, is also tolerated with the L25 linker but not with a shorter spacing region (**Fig. 5-4i**). Moving forward, a 25-residue flexible linker should be the default choice for fusing novel protein domains to the TlpA C-terminus when the application permits such an extended configuration.

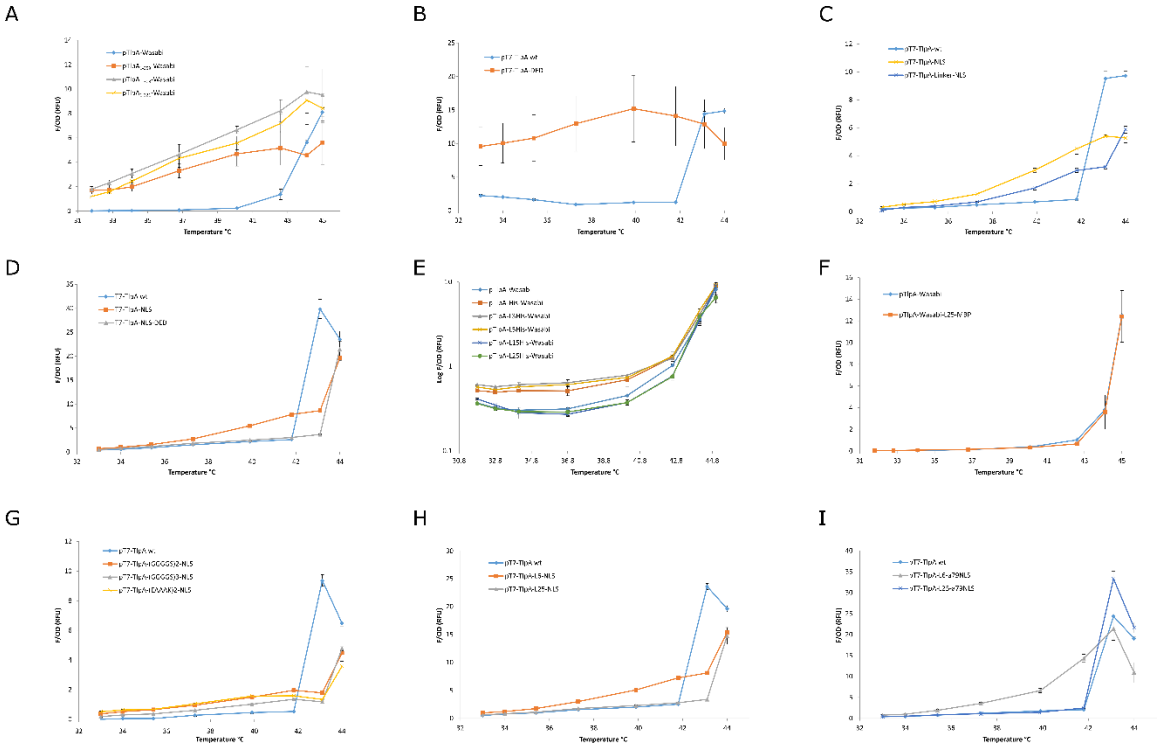

Figure 5-4: Tolerance of TlpA to Structural Perturbations. a) Thermal gene expression of bacteria carrying the standard TlpA-gated GFP expression reporter plasmid reporter in Chapter 3. The wild type TlpA demonstrates cooperative unbinding at a critical temperature centered around 44 °C as described previously, while truncations of the C-terminal 13, 63, or 150 residues (corresponding to the Koski *et al* annotations of the unstructured tail, third coiled-coil segment, and large inter-coil interruption, respectively). All truncations result in repressors displaying poor repression and non-cooperative thermal transitions. **b**) Fusion of TlpA to an Asp-Glu-Asp sequence at its C-terminus significantly inhibits the ability of the protein to repress its cognate promoter. **c**) Fusion of TlpA the SV40 NLS (PKKKRKV), either directly at the C-terminus or spaced by a short SLGSGS linker, promotes transcriptional leakage and abrogates the cooperativity of TlpA unfolding. **d**) Addition of an acidic Asp-Glu-Asp sequence to the TlpA-SLGSGS-NLS construct, separated from the NLS by a Gly-Ser liner, appears to stabilize TlpA repression, perhaps via associating with the basic charges on the partner TlpA strand. **e**) Thermal expression profile of TlpA variants with C-terminal His_6 tags spaced fused directly at the C-terminus or with linkers GGS (L3), GGGGS (L5), $(GGGGS)_3$ (L15), or $(GGGGS)_5$ (L25). While short linkers result in tag-induced inhibition of promoter repression, the L15 linker stabilizes the dimer at temperatures above 34.1 °C and the L25 linker stabilizes the tag at all temperatures. **f**) Thermal expression profile of TlpA compared to a variant with the large globular protein MBP fused at the C-terminus via the $(GGGGS)_5$ linker reveals no significant alteration in repression. **g**) TlpA variants fused to the SV40 NLS at the C-terminus, spaced by intermediate-length flexible linkers $(GGGGS)_2$ or $(GGGGS)_3$ or with the rigid α-helical linker $(EAAAK)_2$. The intermediate linkers are unable to rescue TlpA repression and cooperativity. **h**) Thermal expression profile of wild type TlpA compared to variants with the SV40 NLS fused at the C-terminus via a GGGGS or $(GGGGS)_5$ linker. The long flexible linker is able to tolerize the TlpA protein to the presence of the cationic NLS. **i**) Fusion of the alternative NLS a79 to the C-terminus of TlpA is disruptive when spaced by a SLGSGS but cooperativity and repression is recovered when separated by the L25 linker. *Note that panels **b**, **c**, **d**, **g**, **h**, and **i** utilize an alternative circuit construction in which a T7 promoter is positioned 5' to the TlpA operator/promoter.* All plots represent the mean of N = 3 +/- SEM.

In contrast to the C-terminus, N-terminal analysis of TlpA is difficult via a transcriptional readout due to the required presence of the DNA binding domain in this region. Previous analysis by Hurme et al[13] demonstrated via gel shift that internal deletions in the non-coiled-coil N-terminal domain (TlpA Δ31-43 and Δ61-43) result in loss of DNA binding whereas, surprisingly, the Δ165-320 mutant retained DNA binding (although temperature-dependence was not tested). We tested if the protein is able to accommodate the charged SV40 NLS as an insert between the putative DNA binding domain (residues 1-68) and the coiled-coil domain (residues 69-371) and found that this modification was not tolerated (**Fig. 5-5a**). Surprisingly, circular dichroism spectroscopy analysis of the TlpA coiled coil domain demonstrated that while fusion of a DED tag to the C-terminus destabilizes the protein, such modification of the N-terminus is much better tolerated (**Fig. 5-5b**). Notably, the thermal transition of the C-terminally-tagged variant remains switch-like, albeit with a loss of cooperativity. This suggests that the genetic repression assay may suffer from a minimal threshold of binding ability below which the protein fails to activate in a switch-like manner regardless of the behavior of its coiled-coil domain. Additionally, the near-wild type melting profile of the N-terminally DED-tagged coiled-coil domain suggests that the junction between the DNA binding domain and the coiled-coil domain strongly influences the ability of the protein to repress its promoter and that this geometry, rather than the thermostability of the cold-coil, may be disrupted in the N-terminal NLS fusion shown in **Fig. 5-5a**. To further investigate the effects of N-terminal modification, we swapped the DNA binding domain of TlpA for that of the Tet repressor, another dimerization-dependent DNA binding protein, and assayed its ability to repress the cognate TetR promoter. We fused the TetR DBD at various points within the N-terminal domain of TlpA (**Fig. 5-5c**). All variants

generated a similar reporter gene expression curve regardless of the fusion site chosen. Comparison of one variant to a repressor consisting of only the TetR DNA binding domain with no dedicated dimerization domain (**Fig. 5-5d**) also showed a similar curve, suggesting that fusion of TlpA provides no stabilization beyond the endogenous propensity of the TetR DBD to dimerize at high concentrations. The DNA specificity of coiled-coil DNA-binding proteins has previously been redirected via fusion of the λ cI DBD to the constitutive coiled-coil GCN4[55]. However, in our bacterial thermal transcriptional assay, constructs with cI DBD-TlpA fusion repressors (and also the cI DBD-GCN4 control) demonstrated no fluorescence above background at any temperature (**Fig. 5-5e**). It should be noted that, in contrast to its use in the literature to gate expression from the lambda P_R promoter[56], we utilized these constructs in the context of the pTcI-Wasabi backbone (Chapter 3) in which expression is driven by the strong P_R/P_L hybrid promoter. Unlike in the case of the isolated P_R, we are unable to clone a stable P_R/P_L-containing plasmid in the absence of a repressor, suggesting that the strong expression from this promoter represents a significant metabolic burden and selects for deletion variants. While the Sanger sequencing chromatograms of the TlpA and GCN4 cI-DBD fusion variants did not indicate any deletions or mutations in the promoter, reporter gene, or repressor, it cannot be ruled out that such an alteration occurred during the course of expression. Moving the chimeric cI/TlpA fusion genes into the literature-reported vector may represent a viable approach to assaying the effects of N-terminal TlpA modifications and mapping this boundary of the TlpA coiled-coil domain.

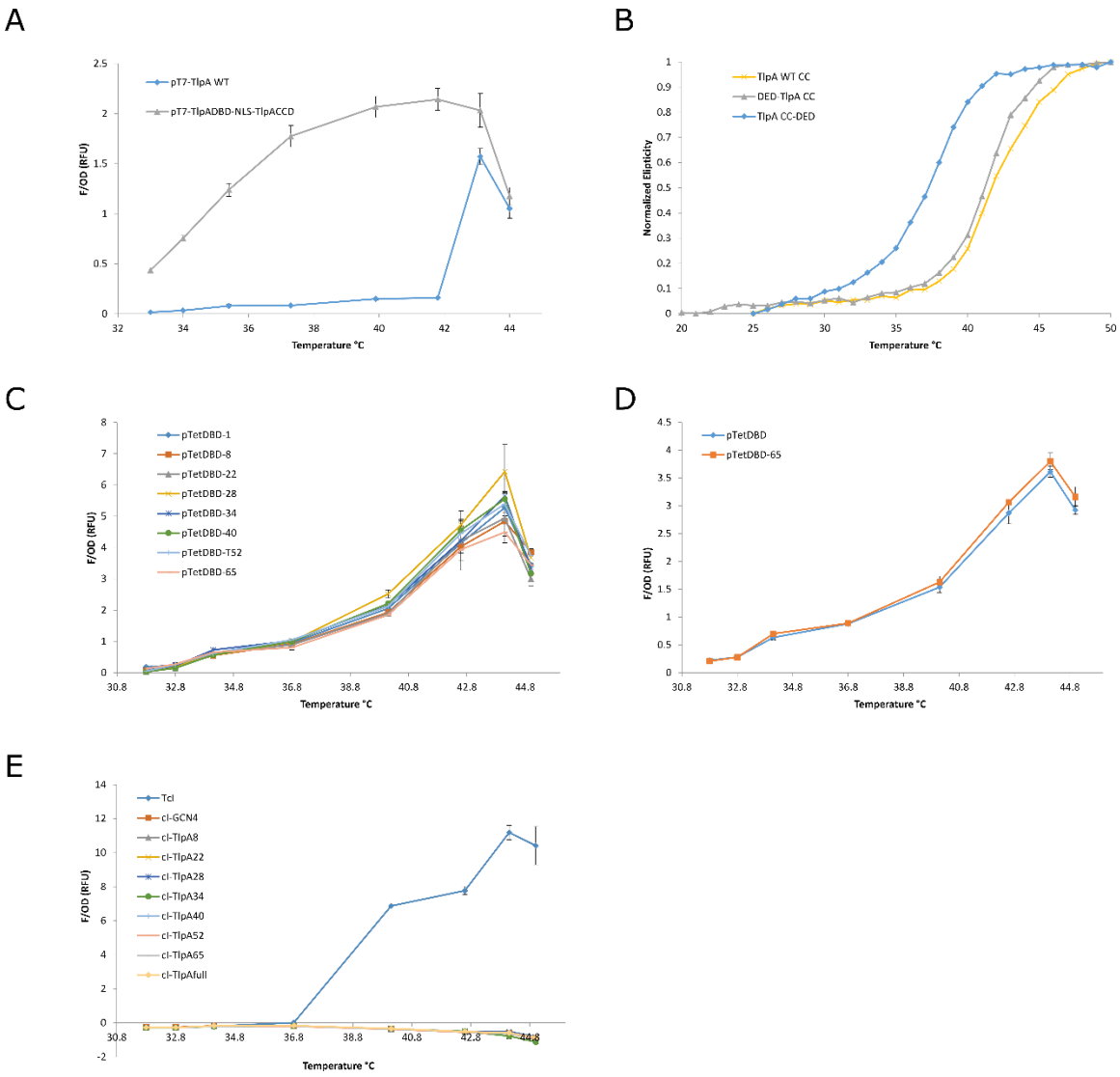

Figure 5-5: N-terminal modification of TlpA. a) Thermal gene expression profile of a TlpA promoter-gated GFP in the presence of wild type TlpA or a variant in which the SV40 NLS is inserted between the putative DNA binding domain and coiled-coil domains (C-terminal to residue 68). **b**) Circular dichroism melting plots tracking ellipticity at 222 nm of the putative TlpA coiled-coil domain (residues 69-359) and variants with the cationic Asp-Glu-Asp tag fused at the N or C-terminus. **c**) Thermal gene expression profiles of a tetA promoter-gated GFP in the presence of chimeric proteins consisting of the TetR DNA binding domain (residues 1-127) fused to TlpA at the indicated positions, spaced by a Gly-Thr linker. **d**) Thermal gene expression profile of ptetA-GFP gated by the TetR-TlpA chimera fused as position 8 within the TlpA DNA binding domain, or by the TetR DNA binding domain in isolation. **e**) Thermal gene expression profile of GFP driven by the tandem pR/pL promoter gated by TcI or a panel of cI DNA binding domain fusions to TlpA variants or to the GCN4 coiled-coil. All gene expression plots represent the mean of N = 3 +/- SEM.

Internal modifications within the TlpA coiled-coil also impact its function. One of the most interesting residues in the protein is its single cysteine, C318, which is predicted to reside at the strand-to-strand interface between TlpA monomers and, as shown in Chapter 4, can be oxidized to form a disulfide. CD Spectroscopic analysis shows that mutation of this residue to a serine destabilizes the coiled-coil, resulting in a lower T_m and a broader transition (**Fig. 5-6a**). Correspondingly, installment of this mutation into the reporter gene regulator circuit results in a significant downshift of the thermal transition (**Fig. 5-6b**). Interestingly, mutating this residue to an alanine, which lacks the terminal sulfhydryl or hydroxyl group, results in an intermediate phenotype, suggesting that while the serine hydroxyls may provide a steric clash leading to destabilization, the sulfhydryls of the cysteine pair may have a stabilizing effect. This stabilization could be due either to disulfide bond formation[57] or from enhanced van der Waals packing[58] of this residue. The lack of a significant crosslinked population in the absence of $CuCl_2$ (Chapter 4) suggests that, at least *in vitro*, the latter effect is dominant. Introduction of oxidants or reductants into the bacterial media during heat shock may elucidate the influence of redox sensing by C318 *in vivo*. Other interesting phenotypes can be observed using circular dichroism spectroscopy or *in situ* control of gene expression. Several residues including glutamate tend to be over-represented at the N-termini of alpha helices and act to stabilize the fold[59]; as such, we investigated if E67, falling just anterior to our annotation of the coiled-coil domain, could influence cooperative unbinding. **Fig. 5-6c** demonstrates little difference in the melting curves of our putative coiled-coil domain fragment ($TlpA_{69-359}$) and the same protein with an N-terminal $V_{66}E_{67}V_{68}$ triplet derived from the preceding N-terminal domain. However, this approach may be useful for future investigation; other residues such as proline are also enriched near the N-termini of helices

and the stretch of $TlpA_{60-65}$ contains two proline residues; comparative stability analysis of fragments containing one or both of these residues may aid in elucidation of the N-terminal helix cap (and thus a suitable fusion point at the N-terminus of the coiled-coil). Figure **5-6C** also shows that a sub-fragment of the coiled-coil domain truncated anterior to the interruption predicted by the COILS server (see **Fig. 5-1**) maintains its ability to unfold cooperatively, albeit at a lower thermal threshold and with weaker cooperativity than its intact counterpart. This fragment may be amenable to stabilization via random mutagenesis and selection (Chapter 3) for use as a fusion tag, wherein its shorter length relative to the wild type TlpA may confer advantages such as conforming to viral packaging limits and decreasing the probability of inducing a penalty to protein folding or expression. The weaker cooperativity of the fragment would also need to be repaired. As demonstrated in **Fig. 3-2B**, error-prone PCR variants of TlpA display a range of switching sharpness phenotypes, suggesting that this property is, like the T_m, amenable to optimization. Furthermore, a small sub-screen of alanine mutants targeting histidine residues predicted by COILS to pack into the strand-strand interface (**Fig. 5-6d**) revealed variant H254A, which demonstrated activation over an apparent span of only 1.5 °C. It would be interesting to determine if installment of this mutation into the truncated $TlpA_{69-276}$ fragment could counteract its apparent length-dependent penalty to switching sharpness. Much work remains to be done in elucidating the sequence determinants of TlpA behavior using rational truncations and mutagenesis. However, without structural data to guide engineering, such information will be invaluable in generating well-behaving TlpA fusions and even the limited scope of the work performed thus far has yielded useful variants for future applications.

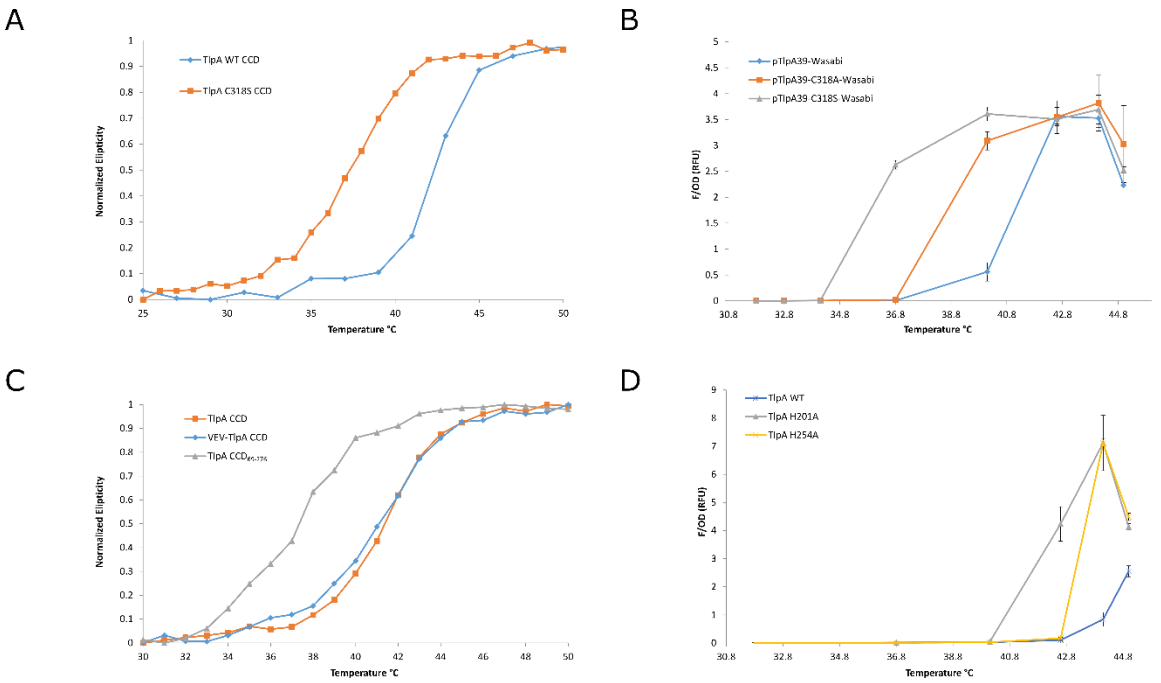

Figure 5-6: Internal modifications of TlpA a) Circular dichroism melting plots tracking ellipticity at 222 nm of the wild type TlpA coiled-coil fragment (residues 69-359) or a variant with the C318S mutation. **b**) Thermal gene expression profile of GFP driven by the pTlpA promoter in the presence of $TlpA_{39}$ or C318 mutants to alanine or cysteine. **c**) Circular dichroism melting plots tracking ellipticity at 222 nm of the TlpA coiled-coil fragment or structural derivatives VEV-TlpA CCD (TlpA residues 66-359) and the TlpA $_{69\text{-}276}$ variant corresponding to the sequence N-terminal to the large coiled-coil interruption predicted by Koski et al. **d**) Thermal gene expression profiles of pTlpA-driven GFP gated by wild type TlpA or core histidine mutants H201A and H254A. Note the unusually sharp transition displayed by the H254A variant. All gene expression plots represent the mean of N = 3 +/- SEM.

5.6: Local Structural Deformation and Activity Modulation

Many of the potential applications for TlpA as a modular bioswitch rely on the ability to fuse one or more proteins of interest to the coiled-coil dimer. To effectively realize this strategy it is important to understand the dynamics of the fusion points; i.e. the behavior of the N or C-termini of the TlpA strands. Coiled-coil denaturation often initiates via “fraying” from the ends of the molecule[60], indicating that local perturbations in these regions precedes global conformational shifts. This local variation in melting threshold has implications for designing

functional protein fusions to TlpA; for example, co-positioning of an enzyme with a corresponding inhibitor will be dependent on the thermal stability of its terminus of fusion rather than on the overall stability of the TlpA dimer or of the other terminus roughly 40 nm distant (**Fig. 5-7a**). Modifications to the termini of the coiled-coil, such as installation of residues that effectively cap the electric dipoles of the helices, may mitigate the fraying effect[61]. The methods described in the preceding section, while useful in assaying the overall behavior of the thermoswitch, are unable to provide information on about this specific aspect of denaturation. Circular dichroism spectroscopy reports on the overall α-helical content of the protein but cannot differentiate between local transitions at the termini vs. internal locations. The shallow linear increase in ellipticity with rising temperature that occurs prior to the main melting transition of coiled-coils is thought to result from fraying at the termini[62], but the technique cannot pinpoint the location at which this fraying occurs. In contrast to CD spectroscopy, the *in vivo* assay for TlpA-mediated transcriptional control is intrinsically dependent on the local stability of TlpA at the N-terminus; however, the dimer-stabilizing effects of DNA binding[63] are likely to mask local fraying (and may account for the lower pre-transition slope demonstrated by the pTlpA-Wasabi circuit and its derivatives relative to the CD spectrum of the purified TlpA protein). While a protein-ligand fusion will provide its own energetic stabilization to the complex if the k_D of the pair is measurable, the relative ΔG of this association may not match that of DNA-DBD binding and as such it would be useful to understand the dynamics of the coiled-coil terminus in isolation.

We have investigated several proximity-based optical approaches such as Forster Resonance Energy Transfer (FRET)[64], Proximity Imaging fluorescence (PRIM)[65], dimerization-

dependent fluorescence (ddXFP)[66], and split luciferase complementation (NanoBiT)[67], for determining the effects of local thermal perturbations to the TlpA structure. We first investigated the use of chemical fluorophores conjugated to the N-terminus of the TlpA coiled-coil. We utilized an N-terminal cysteine fusion to the putative coiled-coil fragment (Met-Cys-TlpA$_{69-359}$) and functionalized it with one of two maleimide-conjugated Alexa fluorescent dyes containing the spectral overlap necessary for FRET to occur. We reasoned that the internal C318 of TlpA is packed into the interface and would therefore be inaccessible for dye labeling, granting selective tracking of the labeled N-terminus. To correct for thermal effects on the dye itself we employed the method of Saccà et al[68], tracking emission intensity of the donor in the presence or absence of the acceptor. Using this approach, we computed the curve shown in **Fig. 5-7b**, which demonstrates a characteristic melting sigmoid with a slightly broader transition and lower T_m than the bulk melting profile observed by CD spectroscopy in **Fig. 5-5b**. While it is tempting to draw conclusions about the fraying behavior of the N-terminus from this data, further validation must be performed to assess potential technical challenges. One such challenge is in understanding the cause of sample-to-sample variation. In **Fig. 5-7c**, the FRET ratio is computed via the Saccà method from pairwise comparison of two wells containing donor-labeled TlpA and two wells containing a mix of donor and acceptor-labeled strands. The two different donor wells produce curves of varying switching sharpness, and it will be important to investigate possible causes of this variability, such as protein denaturation or aggregation, differential labeling efficiency, or potentially partial labeling of the internal cysteine. The latter issue may be circumvented by capitalizing on the single tryptophan residue present in the TlpA N-terminal domain at position 46, which can be directly utilized as a chemical handle via a

recently developed selective coupling reaction[69] or replaced with an azide-containing derivative for facile click labeling[70]. A further complexity, shown in **Fig. 5-7d**, is that despite producing similar curves after normalization, the raw FRET values are quite different between the four possible cross-pairings between two replicates. These differences could also be caused by the aforementioned factors but must be accounted for prior to drawing conclusions for this assay. A further complexity is the potential for thermal effects on dye fluorescence, and therefore on the FRET ratio itself. While the Saccà FRET formula accounts for dye-specific changes in intensity by background subtracting the signal from a reference donor fluorophore in the absence of the acceptor, temperature-induced changes to dye fluorescence may influence spectral overlap and the corresponding FRET efficiency. Therefore, dyes should be selected to minimize thermal effects. As shown in Figure **5-7E**, both the Alexa 546 donor and the Alexa 594 acceptor demonstrate changes in signal intensity upon thermal cycling. While Alexa 594 is relatively stable, displaying a 7% change in signal over four cycles between 25 °C and 50 °C and a 3.5% change within a single cycle, the Alexa 546 molecule shows a drastic 28% signal increase over the full experiment (9% within a single cycle). Both dyes show a characteristic drop in signal intensity as temperature increases followed by a return to a higher baseline upon cooling, resulting in overall signal growth over multiple temperature cycles. Importantly, the FRET ratio for free dye molecules shows no sign of a cooperative transition as a function of temperature (**Fig. 5-7f**) and has a smaller magnitude than the protein FRET signal at the same molecular concentration, suggesting that the transition observed with the dye-labeled protein is indeed induced by a conformational change.

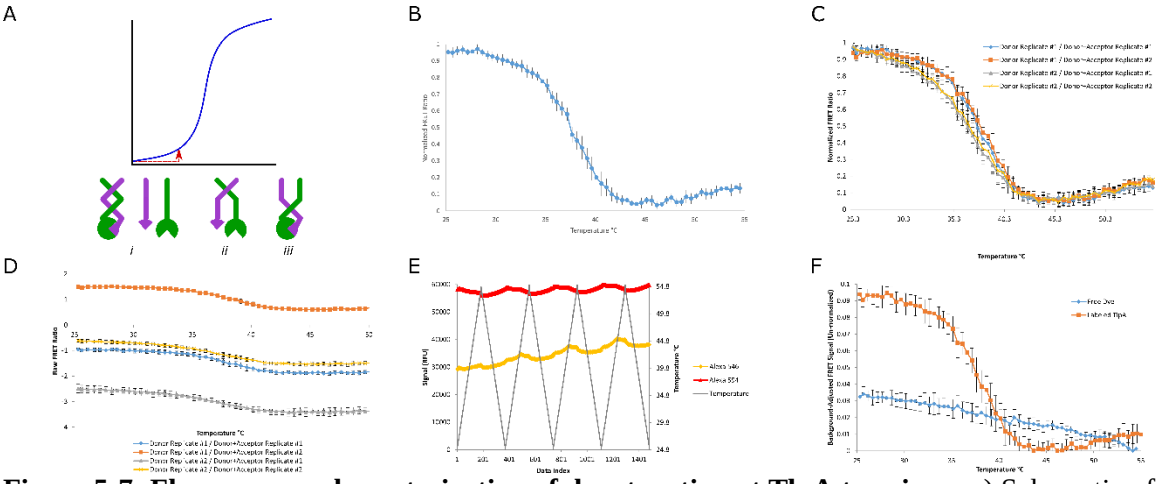

Figure 5-7: Fluorescence characterization of denaturation at TlpA terminus. a) Schematic of possible interpretations of the pre-transition increase in elipticity observed in circular dichroism analysis of TlpA denaturation. This increase can correspond to *i*: a mixed population of fully coiled dimers and fully uncoiled monomers, *ii*: partial uncoiling of TlpA at one terminus, which could potentially impact the dimerization of a locally fused protein, *iii*: partial uncoiling of TlpA at a terminus distal to a potential fusion protein which would not be impacted by the local denaturation. **b**) FRET melting curve computed according to the method of Saccà et al for the TlpA coiled coil fragment with a cysteine residue inserted at position 2 and fused to Alexa 546 or Alexa 594-maleimide conjugates. Data represents the mean of N = 2 donor wells and N = 2 donor/acceptor wells. **c**) FRET melting curve of the four possible combinations of donor and donor/acceptor wells averaged over three consecutive thermal ramps. **d**) The same data as in panel C, but with normalization omitted, demonstrating variable raw signal intensity. **e**) Fluorescence intensity of unreacted Alexa 546 or 594-maleimide conjugates over four thermal cycles between 25 and 55 °C. **f**) Comparison of non-normalized FRET intensity of TlpA-conjugated Alexa fluors or free dyes, averaged over there consecutive thermal cycles.

5.7: On the Concentration-Dependence of TlpA Dissociation

Some engineering applications may require precise control of the TlpA thermal setpoint. As previously reported in the literature, we observed that the melting temperature of TlpA is concentration dependent (**Fig. 5-8a**) and shifts by nearly 3 °C above 1 μM (**Fig. 5-8b**). While the strength of *tlpA* gene expression governs the protein concentration at a bulk level, cell-to-cell variability in protein level can be significant especially for systems without feedback inhibition[71]. To begin addressing this concern, we have investigated the possibility of generating covalent TlpA dimer fusions such that, regardless of the absolute protein

concentration in solution, local TlpA strand concentration could not fall below a minimum set by the linker length. Because the TlpA coiled-coil dimerizes in parallel orientation, a linker between the C-terminus of one strand and the N-terminus of its partner would need to span the predicted 30-40 nm length of the protein. Such a linker may be difficult to clone and would waste a significant amount of sequence space in a viral vector. Instead, we investigated the possibility of harnessing the SpyCatcher/SpyTag system for generating covalent isopeptide bonds spontaneously between two separately expressed proteins[72]. Structural modeling of a coiled-coil fused to the SpyCatcher domain predicted that the linker between the partner strand and its cognate SpyTag would need to span approximately 13 Ångstroms (**Fig. 5-8c**). We therefore constructed a variant of TlpA fused at the C-terminus to SpyCatcher and also built partner variants in which the TlpA is separated from the SpyTag moiety by Gly_3, Gly_5, and Gly_7 linkers. We found that the resulting constructs produced soluble proteins and that isopeptide bond formation occurred freely for all three variants (**Fig. 5-8d**). Unfortunately, the strong β-sheet component of the SpyCatcher domain interferes with circular dichroism analysis of the resulting constructs. Future investigation may be performed using TlpA-gated gene expression analysis, wherein the TlpA may be driven by a weak inducible promoter in a non-feedback configuration to determine its ability to repress its cognate promoter at increasingly low protein copy numbers.

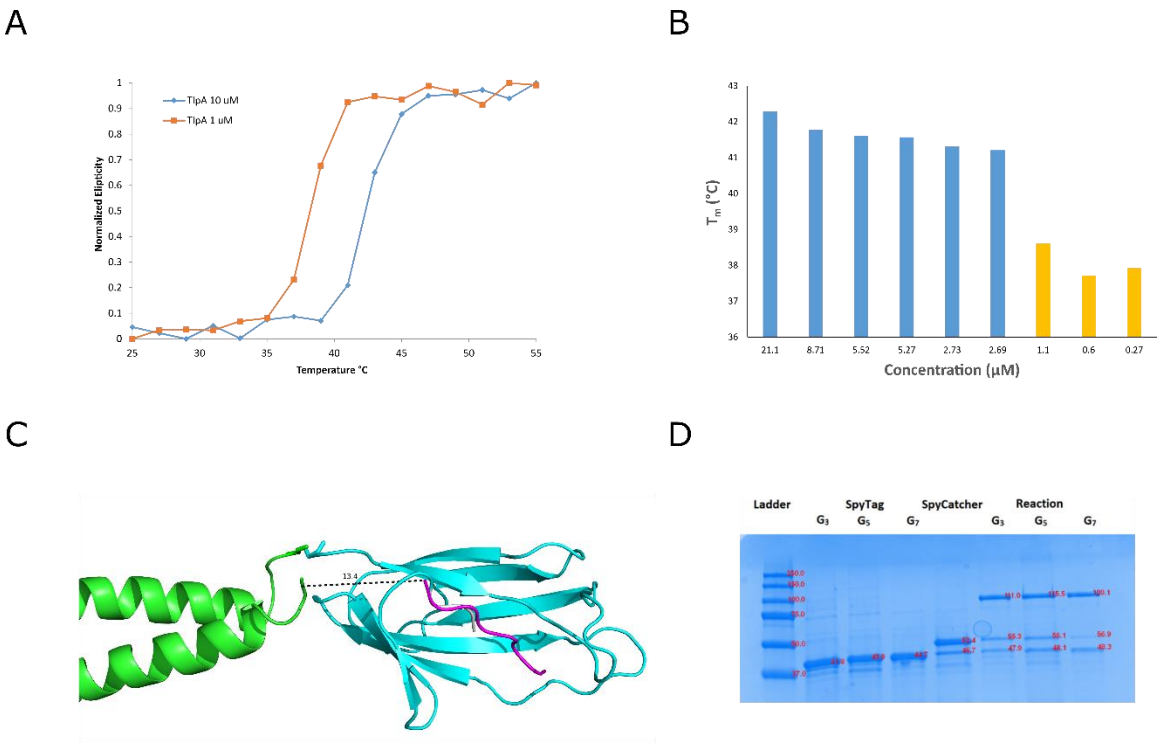

Figure 5-8: Concentration-dependence of TlpA Dissociation. a) Circular dichroism melting curves of the TlpA coiled-coil fragment at 10 μM and 1 μM concentration. Note the shift in T_m. **b**) T_m values computed from CD melting curves of the TlpA coiled-coil fragment at a range of concentrations between 21.1 and 0.27 μM. **c**) Structural modeling of a coiled-coil (Geminin, PDB 4BRY) fused to the SpyCatcher/SpyTag covalent complex (PDB 4MLI). **d**) Coomassie stained SDS-PAGE of *E. coli* lysate demonstrating the shift of unreacted TlpA-SpyTag (36 kDa) and TlpA-SpyCatcher (45 kDa) to a 91 kDa covalent fusion.

5.8: Discussion

The modular and simple structure of TlpA suggests that it could be functionalized and employed for a multitude of applications, following a developmental trajectory similar to that of chemically and optically inducible dimerization systems. Reaching this objective will require robust demonstration that TlpA is functional as a fusion to a variety of protein

domains including signaling proteins and enzymes. To date, the ability to fuse TlpA to proteins of interest has been hampered by a lack of concrete structural data. In the absence of an atomic resolution structure or firm evidence for the boundaries of the coiled-coil domain, TlpA domain fusions must begin from one or several educated inferences regarding the optimal junction site. High-resolution structures generated via X-ray crystallography or electron microscopy, in addition to fine-grained truncation and mutagenesis studies using circular dichroism spectroscopy or native transcriptional modulation in bacteria, may enable the production of functional and robust TlpA fusion proteins.

Thermal control remains the most accessible method to modulate biological function noninvasively and at depth within large animal models and in human patients (see Chapter 2). The lack of synthetic biology tools to confer temperature-responsive behavior to arbitrary proteins of interest greatly limits the range of applications available to this technology both in fundamental research and in the clinic. In prokaryotes, the TlpA and TcI thermal bioswitches have enabled ultrasound and fever-responsive transcription (Chapter 3). In the future, this technology may enable physicians to activate microbial therapeutics in a “point and click” fashion to increase the safety and efficacy of these treatments. In mammalian cells, such control is currently limited to heat shock promoters, which suffer from crosstalk with non-thermal stress pathways and a lack of temperature tunability. The advances described herein in using TlpA as a modular thermal bioswitch to control protein-protein interactions (Chapter 4) demonstrate the feasibility of imparting a novel, noninvasive control axis to any number of biological pathways of interest. Control of sub-cellular localization or inducible association with biological inhibitors of function can enable biomodulation in arbitrary cell

types, including in mammalian cells, on timescales of seconds or minutes. In the future, functional analysis of TlpA variants using platforms such as those discussed in this chapter can inform the design of bioactive protein-TlpA chimeras for scientific and clinical applications. We expect that our prototype TlpA-based bioswitch will serve as the foundation of a widespread method to utilize ultrasound-based or physiological hyperthermia as a new and important method to study biological processes, and potentially to enable the development of safer biological therapies.

5.9: Methods

Plasmid Construction and Molecular Biology

Plasmids were designed using SnapGene (GSL Biotech) and assembled via KLD mutagenes, Gibson Assembly, or restriction/ligation using enzymes from New England Biolabs. All plasmids and sequences will be uploaded as a supplemental file. After assembly, constructs were transformed into NEB Turbo, NEB10β, or NEB Stable *E. coli* (New England Biolabs) for growth and plasmid preparation. Thermal gene expression assays were performed in NEB10β. Fluorescent reporters and transcription repression genes and circuits were obtained from our previous work[1].

Thermal Regulation Assay

Determination of temperature-dependent gene expression was performed as described previously[1]. Saturated precultures were diluted to OD_{600} = 0.1 and propagated at 30 °C until reaching OD_{600} = 0.3 as measured via Nanodrop 2000c (Thermo Scientific). 25 uL aliquots were dispensed into PCR tubes with transparent caps (Bio-Rad) and incubated for 12 hours

in a thermal gradient using a Bio-Rad C1000 Touch thermocycler. After thermal stimulus, fluorescence was measured using a Stratagene MX3005p qPCR (Agilent), after which cultures were diluted 4x, transferred into microplates (Costar black / clear bottom), and measured for OD_{600} using a Molecular Devices SpectraMax M5 plate reader. The background-corrected F/OD is reported as described previously[1].

Protein Expression

pET26b-based expression constructs were transformed into BL21-DE3 *E. coli* and grown on kanamycin-selective plates. Saturated overnight cultures were diluted 1 mL into 400 mL expression cultures and induced with a final IPTG concentration of 1 mM at OD_{600} = 0.6. After 24 hours of expression at 25 °C, cultures were harvested by centrifugation using a JLA-16.250 rotor (Beckman Coulter) at 6,000 rpm and 4 °C for 8 minutes. Pellets were lysed using the detergent Solulyse in Tris Buffer (Genlantis) and debris was pelleted by centrifugation at 35,343 rcf in a JS-24.38 rotor (Beckman Coulter). Polyhistidine-tagged proteins were purified on an AKTA purifier (GE Healthcare) using 1 mL cOmplete columns (Roche) and buffer exchanged into 1x PBS (Corning) using Zeba 7K MWCO desalting columns (Thermo Fisher Scientific). Concentration was determined using the Pierce 660nm Protein Assay (Thermo Fisher Scientific) and proteins were stored at 4 °C until use.

Circular Dichroism Spectroscopy

CD melting curves were taken using an Aviv Circular Dichroism Spctrophotometer (Model 60DS) at 222 nm with 0.1 minute equilibration time and 5 second averaging time. Purified proteins were diluted to 10 µM (unless specified otherwise) in 1x PBS and measured in a 1 mm quartz cuvette.

Protein FRET measurement

10 mM stocks of Alexa 546 and Alexa 594-maleimide conjugates (Thermo Fisher Scientific) were prepared in anhydrous DMSO (Sigma Aldrich). Purified Met-Cys-TlpA was diluted to 2 µM in 1x PBS and split into two 50 uL aliquots. 10 mM Alexa-maleimide was added so as to achieve 10-fold molar excess of dye:protein. Reactions were performed overnight at room temperature. Dye was removed via filtration through 7,000 MWCO Zeba column. Labeled proteins were mixed in equal volumes (10 uL each species), heated to 45 °C for 10 minutes in an Eppendorf Thermomixer to promote strand exchange, and then cooled down to room temperature. For the donor-only sample required for calculating the temperature-corrected FRET ratio, the Alexa 546-labeled protein was mixed with 1x PBS instead of the Alexa 594-labeled variant. The 20 uL samples were transferred to optically clear PCR strips (Bio Rad) and donor fluorescence as a function of temperature was measured on the HXRX channel of the Stratagene MX3005p qPCR instrument.

5.10: References

1. Piraner, D. I., Abedi, M. H., Moser, B. A., Lee-Gosselin, A. & Shapiro, M. G. Tunable thermal bioswitches for in vivo control of microbial therapeutics. *Nat. Chem. Biol.* **13**, 75–80 (2017).
2. Szostak, M. P. *et al.* Bacterial ghosts : non-living candidate vaccines. **44**, (1996).
3. Valdez-Cruz, N. a, Caspeta, L., Pérez, N. O., Ramírez, O. T. & Trujillo-Roldán, M. a. Production of recombinant proteins in E. coli by the heat inducible expression system based on the phage lambda pL and/or pR promoters. *Microb. Cell Fact.* **9**, 18 (2010).
4. Spencer, D. M., Wandless, T. J., Schreiber, S. L. & Crabtree, G. R. Controlling signal transduction with synthetic ligands. *Science (80-.).* **262**, 1019–1024 (1993).
5. Liang, F.-S., Ho, W. Q. & Crabtree, G. R. Engineering the ABA Plant Stress Pathway for Regulation of Induced Proximity. *Sci. Signal.* **4**, 1–9 (2011).
6. Miyamoto, T. *et al.* Rapid and orthogonal logic gating with a gibberellin-induced dimerization system. *Nat. Chem. Biol.* **8**, 465–470 (2012).
7. Hill, Z. B., Martinko, A. J., Nguyen, D. P. & Wells, J. A. Human antibody-based chemically induced dimerizers for cell therapeutic applications. *Nat. Publ. Gr.* (2017). doi:10.1038/nchembio.2529
8. DeRose, R., Miyamoto, T. & Inoue, T. Manipulating signaling at will: chemically-inducible dimerization (CID) techniques resolve problems in cell biology. *Pflügers Arch. - Eur. J. Physiol.* **465**, 409–417 (2013).
9. Shimizu-Sato, S., Huq, E., Tepperman, J. M. & Quail, P. H. A light-switchable gene promoter system. *Nat. Biotechnol.* **20**, 1041–1044 (2002).
10. Yazawa, M., Sadaghiani, A. M., Hsueh, B. & Dolmetsch, R. E. Induction of protein-protein interactions in live cells using light. *Nat. Biotechnol.* **27**, 941–945 (2009).
11. Kawano, F., Suzuki, H., Furuya, A. & Sato, M. Engineered pairs of distinct photoswitches for optogenetic control of cellular proteins. *Nat. Commun.* **6**, 6256 (2015).
12. Koski, P. *et al.* A new alpha-helical coiled coil protein encoded by the Salmonella typhimurium virulence plasmid. *J. Biol. Chem.* **267**, 12258–12265 (1992).
13. Hurme, R., Berndt, K. D., Namork, E. & Rhen, M. DNA Binding Exerted by a Bacterial Gene Regulator with an Extensive Coiled-coil Domain. *J. Biol. Chem.* **271**, 12626–12631 (1996).
14. Sadowski, M. I. & Jones, D. T. The sequence–structure relationship and protein function prediction. *Curr. Opin. Struct. Biol.* **19**, 357–362 (2009).
15. Lehrer, S. S. & Qian, Y. Unfolding/refolding studies of smooth muscle tropomyosin. Evidence for a chain exchange mechanism in the preferential assembly of the native heterodimer. *J. Biol. Chem.* **265**, 1134–1138 (1990).
16. Lehrer, S. S. & Stafford, W. F. Preferential assembly of the tropomyosin heterodimer: equilibrium studies. *Biochemistry* **30**, 5682–5688 (1991).
17. Krishnan, V. & Rupp, B. Macromolecular Structure Determination: Comparison of X-ray Crystallography and NMR Spectroscopy. in *eLS* (John Wiley & Sons, Ltd, 2012). doi:10.1002/9780470015902.a0002716.pub2
18. Murata, K. & Wolf, M. Cryo-electron microscopy for structural analysis of dynamic biological macromolecules. *Biochim. Biophys. Acta - Gen. Subj.* **1862**, 324–334 (2018).
19. Frueh, D. P., Goodrich, A. C., Mishra, S. H. & Nichols, S. R. NMR methods for structural studies of large monomeric and multimeric proteins. *Curr. Opin. Struct. Biol.* **23**, 734–739 (2013).
20. Kumar, D. *et al.* Pseudo 5D HN(C)N experiment to facilitate the assignment of backbone resonances in proteins exhibiting high backbone shift degeneracy. *Chem. Phys.* **441**, 144–151 (2014).

21. Li, Y., Berthold, D. A., Gennis, R. B. & Rienstra, C. M. Chemical shift assignment of the transmembrane helices of DsbB, a 20-kDa integral membrane enzyme, by 3D magic-angle spinning NMR spectroscopy. *Protein Sci.* **17**, 199–204 (2008).
22. Hurme, R., Namork, E., Nurmiaho-Lassila, E.-L. & Rhen, M. Intermediate filament-like network formed in vitro by a bacterial coiled coil protein. *J. Biol. Chem.* **269**, 10675–10682 (1994).
23. Martin, T. G. *et al.* Design of a molecular support for cryo-EM structure determination. *Proc. Natl. Acad. Sci.* **113**, E7456–E7463 (2016).
24. Coscia, F. *et al.* Fusion to a homo-oligomeric scaffold allows cryo-EM analysis of a small protein. *Sci. Rep.* **6**, 30909 (2016).
25. Liu, Y., Gonen, S., Gonen, T. & Yeates, T. O. Near-atomic cryo-EM imaging of a small protein displayed on a designed scaffolding system. *Proc. Natl. Acad. Sci.* **115**, 3362–3367 (2018).
26. Kato, T., Goodman, R. P., Erben, C. M., Turberfield, A. J. & Namba, K. High-Resolution Structural Analysis of a DNA Nanostructure by cryoEM. *Nano Lett.* **9**, 2747–2750 (2009).
27. Ketterer, P. *et al.* DNA origami scaffold for studying intrinsically disordered proteins of the nuclear pore complex. *Nat. Commun.* **9**, 902 (2018).
28. Kollman, J. M., Pandi, L., Sawaya, M. R., Riley, M. & Doolittle, R. F. Crystal Structure of Human Fibrinogen. *Biochemistry* **48**, 3877–3886 (2009).
29. Bhardwaj, A., Casjens, S. R. & Cingolani, G. Exploring the atomic structure and conformational flexibility of a 320 Å long engineered viral fiber using X-ray crystallography. *Acta Crystallogr. Sect. D Biol. Crystallogr.* **70**, 342–353 (2014).
30. Bhardwaj, A. *et al.* Structural Plasticity of the Protein Plug That Traps Newly Packaged Genomes in Podoviridae Virions. *J. Biol. Chem.* **291**, 215–226 (2016).
31. Whitby, F. G. & Phillips, G. N. Crystal structure of tropomyosin at 7 Angstroms resolution. *Proteins Struct. Funct. Genet.* **38**, 49–59 (2000).
32. McPherson, A. & Cudney, B. Optimization of crystallization conditions for biological macromolecules. *Acta Crystallogr. Sect. F Struct. Biol. Commun.* **70**, 1445–1467 (2014).
33. Müller, I. Guidelines for the successful generation of protein–ligand complex crystals. *Acta Crystallogr. Sect. D Struct. Biol.* **73**, 79–92 (2017).
34. Hurme, R., Berndt, K. D., Normark, S. J. & Rhen, M. A proteinaceous gene regulatory thermometer in Salmonella. *Cell* **90**, 55–64 (1997).
35. Drozdetskiy, A., Cole, C., Procter, J. & Barton, G. J. JPred4: a protein secondary structure prediction server. *Nucleic Acids Res.* **43**, W389–W394 (2015).
36. Lupas, a, Van Dyke, M. & Stock, J. Predicting coiled coils from protein sequences. *Science (80-.).* **252**, 1162–1164 (1991).
37. McDonnell, A. V., Jiang, T., Keating, A. E. & Berger, B. Paircoil2: improved prediction of coiled coils from sequence. *Bioinformatics* **22**, 356–358 (2006).
38. Vincent, T. L., Green, P. J. & Woolfson, D. N. LOGICOIL--multi-state prediction of coiled-coil oligomeric state. *Bioinformatics* **29**, 69–76 (2013).
39. Kirwan, J. P. & Hodges, R. S. Transmission of Stability Information through the N-domain of Tropomyosin Is Interrupted by a Stabilizing Mutation (A109L) in the Hydrophobic Core of the Stability Control Region (Residues 97–118). *J. Biol. Chem.* **289**, 4356–4366 (2014).
40. Beasley, M. Conserved Disruptions in the Predicted Coiled-Coil Domains of Eukaryotic SMC Complexes: Implications for Structure and Function. *Genome Res.* **12**, 1201–1209 (2002).
41. Gunning, P. W., Hardeman, E. C., Lappalainen, P. & Mulvihill, D. P. Tropomyosin - master regulator of actin filament function in the cytoskeleton. *J. Cell Sci.* **128**, 2965–2974 (2015).
42. Mason, J. M., Schmitz, M. A., Muller, K. M. & Arndt, K. M. Semirational design of Jun-Fos coiled coils with increased affinity: Universal implications for leucine zipper prediction and

design. *Proc. Natl. Acad. Sci.* **103**, 8989–8994 (2006).
43. Vorov, O. K., Livesay, D. R. & Jacobs, D. J. Helix/coil nucleation: a local response to global demands. *Biophys. J.* **97**, 3000–9 (2009).
44. Fujiwara, Y., Takeshita, K., Nakagawa, A. & Okamura, Y. Structural Characteristics of the Redox-sensing Coiled Coil in the Voltage-gated H + Channel. *J. Biol. Chem.* **288**, 17968–17975 (2013).
45. Avner, B. S. *et al.* Myocardial infarction in mice alters sarcomeric function via post-translational protein modification. *Mol. Cell. Biochem.* **363**, 203–215 (2012).
46. Gal-Mor, O., Valdez, Y. & Finlay, B. B. The temperature-sensing protein TlpA is repressed by PhoP and dispensable for virulence of Salmonella enterica serovar Typhimurium in mice. *Microbes Infect.* **8**, 2154–62 (2006).
47. Husain, M. *et al.* Redox sensor SsrB Cys203 enhances Salmonella fitness against nitric oxide generated in the host immune response to oral infection. *Proc. Natl. Acad. Sci.* **107**, 14396–14401 (2010).
48. van der Heijden, J., Bosman, E. S., Reynolds, L. A. & Finlay, B. B. Direct measurement of oxidative and nitrosative stress dynamics in Salmonella inside macrophages. *Proc. Natl. Acad. Sci.* **112**, 560–565 (2015).
49. Lee, C., Zhong, L., Mace, T. A. & Repasky, E. A. Elevation in Body Temperature to Fever Range Enhances and Prolongs Subsequent Responsiveness of Macrophages to Endotoxin Challenge. *PLoS One* **7**, e30077 (2012).
50. Habicht, G. S. Body temperature in normal and endotoxin-treated mice of different ages. *Mech. Ageing Dev.* **16**, 97–104 (1981).
51. Altschul, S., Gish, W., Miller, W., Myers, E. & Lipman, D. Basic local alignment search tool. *J. Mol. Biol.* **215**, 403–410 (1990).
52. Deligios, M. Structural and functional genomic analysis of the salmonella enterica host-restricted serotype abortusovis. (Universita Degli Studi di Sassari, 2008).
53. Casutt-Meyer, S. *et al.* Oligomeric Coiled-Coil Adhesin YadA Is a Double-Edged Sword. *PLoS One* **5**, e15159 (2010).
54. Kosugi, S. *et al.* Six classes of nuclear localization signals specific to different binding grooves of importin alpha. *J. Biol. Chem.* **284**, 478–85 (2009).
55. Hu, J. C., O'Shea, E. K., Kim, P. S. & Sauer, R. T. Sequence requirements for coiled-coils: analysis with lambda repressor-GCN4 leucine zipper fusions. *Science* **250**, 1400–3 (1990).
56. Mariño-Ramírez, L., Campbell, L. & Hu, J. C. Screening Peptide/Protein Libraries Fused to the λ Repressor DNA-Binding Domain in E. coli Cells. in *E. coli Gene Expression Protocols* 235–250 (Humana Press, 2011). doi:10.1385/1-59259-301-1:235
57. Yin, X. *et al.* Contribution of Disulfide Bridges to the Thermostability of a Type A Feruloyl Esterase from Aspergillus usamii. *PLoS One* **10**, e0126864 (2015).
58. You, C., Huang, Q., Xue, H., Xu, Y. & Lu, H. Potential hydrophobic interaction between two cysteines in interior hydrophobic region improves thermostability of a family 11 xylanase from Neocallimastix Patriciarum. *Biotechnol. Bioeng.* **105**, n/a-n/a (2010).
59. Aurora, R. & Rosee, G. D. Helix capping. *Protein Sci.* **7**, 21–38 (1998).
60. Dragan, A. I. & Privalov, P. L. Unfolding of a Leucine zipper is not a Simple Two-state Transition. *J. Mol. Biol.* **321**, 891–908 (2002).
61. Fesinmeyer, R. M., Peterson, E. S., Dyer, R. B. & Andersen, N. H. Studies of helix fraying and solvation using 13 C′ isotopomers. *Protein Sci.* **14**, 2324–2332 (2005).
62. Kwok, S. C. & Hodges, R. S. Stabilizing and Destabilizing Clusters in the Hydrophobic Core of Long Two-stranded α-Helical Coiled-coils. *J. Biol. Chem.* **279**, 21576–21588 (2004).
63. Mohana-borges, R. *et al.* LexA Repressor Forms Stable Dimers in Solution. *J. Biol. Chem.* **275**, 4708–4712 (2000).

64. Piston, D. W. & Kremers, G.-J. Fluorescent protein FRET: the good, the bad and the ugly. *Trends Biochem. Sci.* **32**, 407–14 (2007).
65. De Angelis, D. a, Miesenböck, G., Zemelman, B. V & Rothman, J. E. PRIM: proximity imaging of green fluorescent protein-tagged polypeptides. *Proc. Natl. Acad. Sci. U. S. A.* **95**, 12312–6 (1998).
66. Alford, S. C., Ding, Y., Simmen, T. & Campbell, R. E. Dimerization-dependent green and yellow fluorescent proteins. *ACS Synth. Biol.* **1**, 569–575 (2012).
67. Dixon, A. S. *et al.* NanoLuc Complementation Reporter Optimized for Accurate Measurement of Protein Interactions in Cells. *ACS Chem. Biol.* (2015). doi:10.1021/acschembio.5b00753
68. Saccà, B., Meyer, R. & Niemeyer, C. M. Temperature-dependent FRET spectroscopy for the high-throughput analysis of self-assembled DNA nanostructures in real time. *Nat. Protoc.* **4**, 271–85 (2009).
69. Seki, Y. *et al.* Transition Metal-Free Tryptophan-Selective Bioconjugation of Proteins. *J. Am. Chem. Soc.* **138**, 10798–10801 (2016).
70. Italia, J. S., Addy, P. S., Wrobel, C. J. J., Crawford, L. A. & Lajoie, M. J. An orthogonalized platform for genetic code expansion in both bacteria and eukaryotes. *Nat. Chem. Biol.* **13**, 446–450 (2017).
71. Murphy, K. F., Adams, R. M., Wang, X. & Collins, J. J. Tuning and controlling gene expression noise in synthetic gene networks. *Nucleic Acids Res.* **38**, 2712–2726 (2010).
72. Zakeri, B. *et al.* Peptide tag forming a rapid covalent bond to a protein, through engineering a bacterial adhesin. *Proc. Natl. Acad. Sci. U. S. A.* **109**, E690-7 (2012).